Supporting Information

Sheathless Focusing and Separation of Diverse Nanoparticles in Viscoelastic Solutions with Minimized Shear Thinning

Chao Liu,[†, ‡] Baoquan Ding,[//] Chundong Xue,[†, ‡] Yu Tian,[¶] Guoqing Hu,[*†, ‡] and Jiashu Sun[*//]

[†]State Key Laboratory of Nonlinear Mechanics, Beijing Key Laboratory of Engineered Construction and Mechanobiology, Institute of Mechanics, Chinese Academy of Sciences, Beijing 100190, China.

[‡]School of Engineering Science, University of Chinese Academy of Sciences, Beijing 100049, China.

[//]CAS Key Laboratory for Biological Effects of Nanomaterials and Nanosafety, CAS Center for Excellence in Nanoscience, National Center for NanoScience and Technology, Beijing 100190, China.

[¶]State Key Laboratory of Tribology, Tsinghua University, Beijing 100084, China.

*To whom correspondence should be addressed. E-mail: guoqing.hu@imech.ac.cn and sunjs@nanoctr.cn.

Contents:

Relaxation time

The relaxation times for PEO solutions with varying M_w are evaluated by the empirical formula based on capillary breakup extension rheometry (CaBER) measurement: $\lambda = 18\lambda_Z \left(c/c^*\right)^{0.65}$.[1] Here the overlapping concentration $c^* = 0.77/[\eta]$, and the intrinsic viscosity $[\eta]$ is determined by the Mark-Houwink relation, $[\eta] = 0.072 M_w^{0.65}$.[2] Zimm theory predicts the relaxation time as $\lambda_Z = F[\eta] M_w \eta_s / N_A k_B T$, where the prefactor $F = 0.463$, the solvent viscosity $\eta_s = 1\times10^{-3} Pa\cdot s$, N_A is the Avogadro's number and k_B is the Boltzmann's constant.[3] As a result, the relaxation time λ calculated for the PEO solutions of various M_w used in Figure 3 study are listed in Table S-1.

Table S-1. The relaxation times for PEO solutions with varying M_w.

M_w	0.6×10^6g/mol	1×10^6 g/mol	2×10^6 g/mol	4×10^6 g/mol	8×10^6 g/mol
c^*	1877 ppm	1346 ppm	858 ppm	547 ppm	348 ppm
c/c^*	3.2	3.0	3.7	4.6	5.7
λ_Z	0.046 ms	0.11 ms	0.35 ms	1.1 ms	3.3 ms
λ	1.76 ms	4.02 ms	14.8 ms	53.2 ms	185 ms

Numerical prediction of particle trajectories

The elastic lift forces acting on a particle is

$$\mathbf{F}_e = Ca^3 \nabla N_1 \tag{S1}$$

where C is the elastic lift coefficient, a the particle diameter, and N_1 the first normal stress difference defined as $N_1 = \sigma_{11} - \sigma_{22}$, where σ_{11} and σ_{22} are the normal stresses in the flow and velocity gradient directions, respectively. N_1 is calculated as $N_1 = 2\eta_p \lambda \dot{\gamma}^2$ using Oldroyd-B model, here η_p is the polymeric contribution to the solution viscosity[4] and the shear rate $\dot{\gamma}$ is defined as $(2\mathbf{D}:\mathbf{D})^{1/2}$, where $\mathbf{D}$ is the deformation rate tensor and is expressed as $\mathbf{D} = \nabla\mathbf{u}/2 + (\nabla\mathbf{u})^T/2$ ($\mathbf{u}$ is the fluid velocity).

We conduct Lagrangian tracking for predicting the particle trajectories using Fluent (Fluent 6.4, ANSYS Inc.). A steady flow field without particles is first obtained by solving the incompressible Navier–Stokes equations

$$\begin{aligned} \nabla \cdot \mathbf{u} &= 0 \\ \rho(\mathbf{u}\cdot\nabla)\mathbf{u} &= -\nabla p + \eta\nabla^2\mathbf{u} \end{aligned} \tag{S2}$$

where ρ is the fluid density, p the pressure, and η the fluid kinetic viscosity. Based on the solved flow field, particle trajectories are predicted by integrating the force balance of the particle based on Newton's second law of motion

$$\frac{d\mathbf{V}_p}{dt} = \frac{18\eta}{\rho_p a^2}\frac{C_D Re_s}{24}\left(\mathbf{u}-\mathbf{V}_p\right) + \frac{\mathbf{g}(\rho_p-\rho)}{\rho_p} + \frac{1}{2}\frac{\rho}{\rho_p}\frac{d(\mathbf{u}-\mathbf{V}_p)}{dt} + \frac{\mathbf{F}_e}{\frac{1}{6}\pi a^3\rho_p} \tag{S3}$$

where $\mathbf{V}_p$ is the particle velocity, ρ_p the particle density, C_D the drag coefficient, Re_s the relative Reynolds number $Re_s = \rho a\left|\mathbf{u}-\mathbf{V}_p\right|/\eta$, and $\mathbf{g}$ the gravitational acceleration. On the right hand of the force balance equation, the first term is the viscous drag force per unit particle mass. The C_D is calculated using an analytical expression given by Morsi and Alexander[5]

$$C_D = a_1 + \frac{a_2}{Re_s} + \frac{a_3}{Re_s^2} \tag{S4}$$

where a_1, a_2, and a_3 are constants that apply over a wide range of Re_s. The second term is buoyant force that can be neglected for neutrally-buoyant particles. The third term is the virtual mass force arising from the acceleration of the fluid around the particle. The fourth term is the elastic lift, which can be implemented using a user defined function in Fluent (Fluent 6.4, ANSYS Inc.). The diameter a is set to be 100 nm, η, η_p, and λ are 6.9 mPa·s, 5.9 mPa·s and 1.76 ms, respectively, for the PEO solution of $M_w = 0.6\times10^6$ g/mol and $c = 0.6$ wt %, C is 5π/384 which is derived from the analytical model by Ho and Leal.[6] A no-slip boundary condition is imposed on the channel walls. A pressure boundary condition is imposed at the inlet to match the flow rates set in the experiments, while an ambient pressure is set at the outlet.

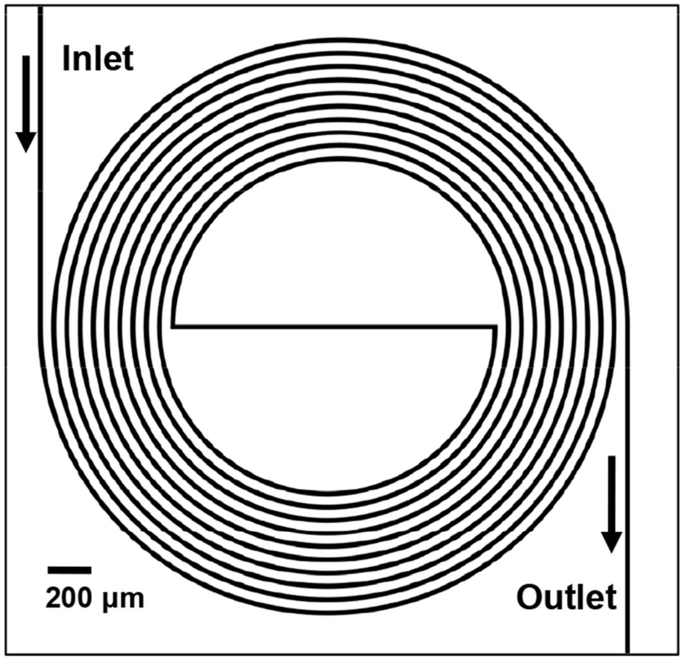

Figure S-1. CAD image showing that the double spiral microchannel consists of 5 loops for each spiral, resulting in a total length exceeding 60 mm. The arrows indicate the flow direction.

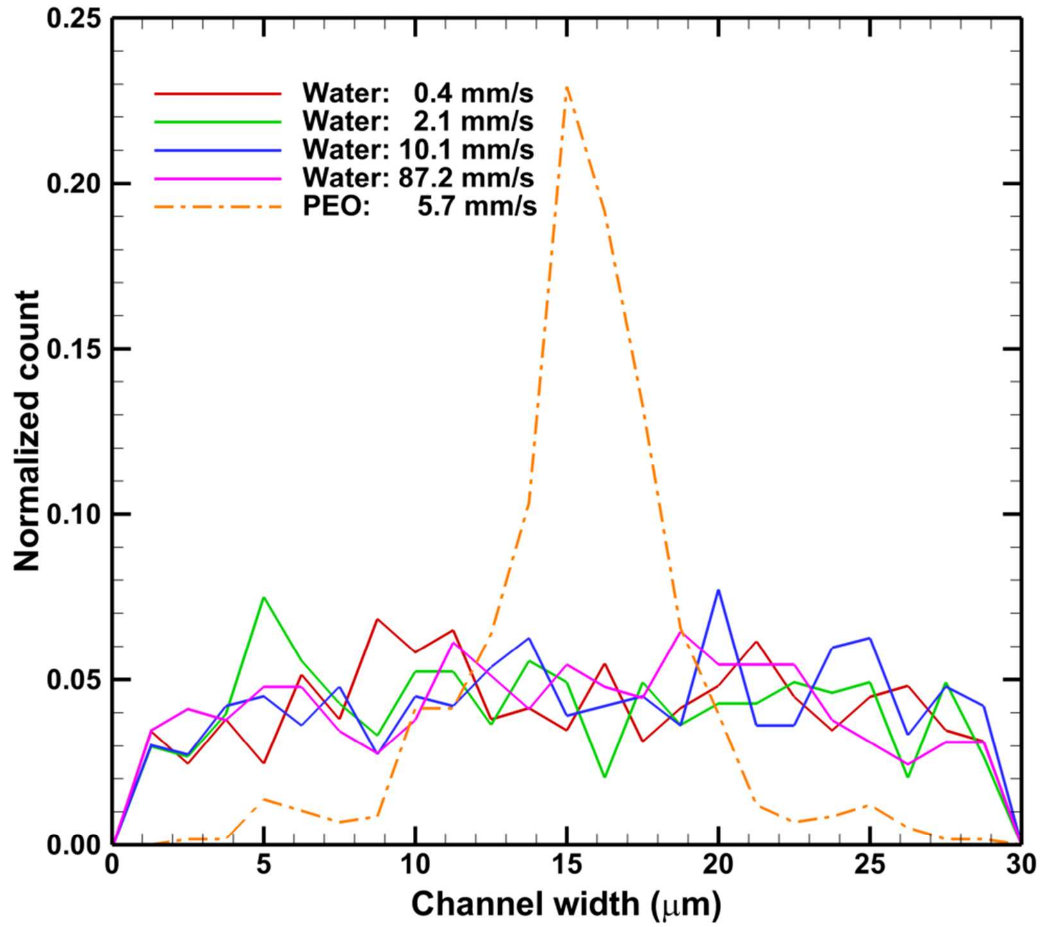

Figure S-2. The spatial distributions of 100 nm particles in deionized water at flow speeds ranging from 0.4 to 87.2 mm/s. The corresponding Reynolds numbers range from 0.0028 to 0.61. The result of the PEO solution of M_w = 6×10^5 g/mol at a flow speed of 5.7 mm/s is also shown for visual comparison.

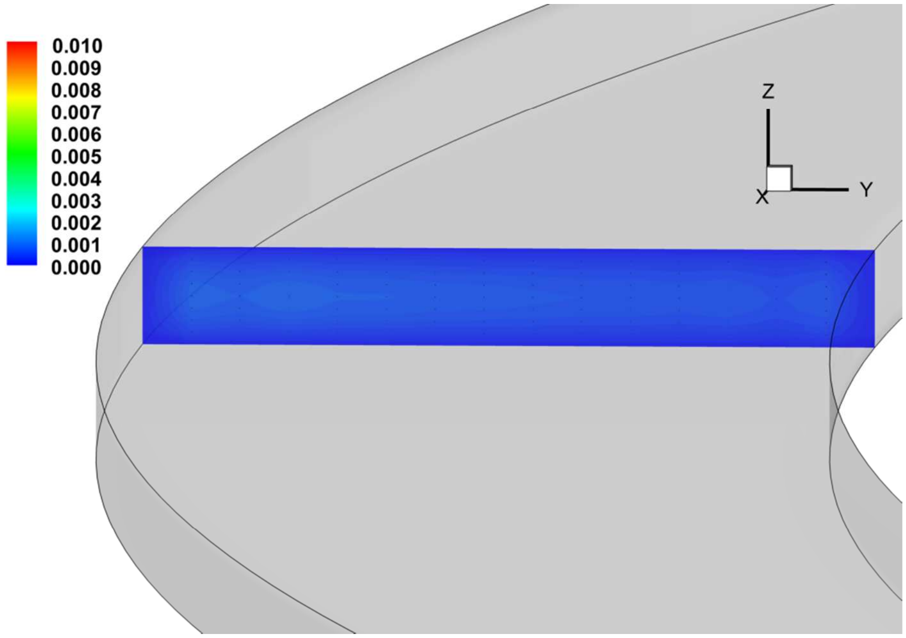

Figure S-3. The ratios of secondary flow velocities to the maximum channel velocity are shown as a contour plot at the cross section of the innermost loop. The maximum velocity is 10 mm/s and the corresponding *De* is 1.3×10^{-3}.

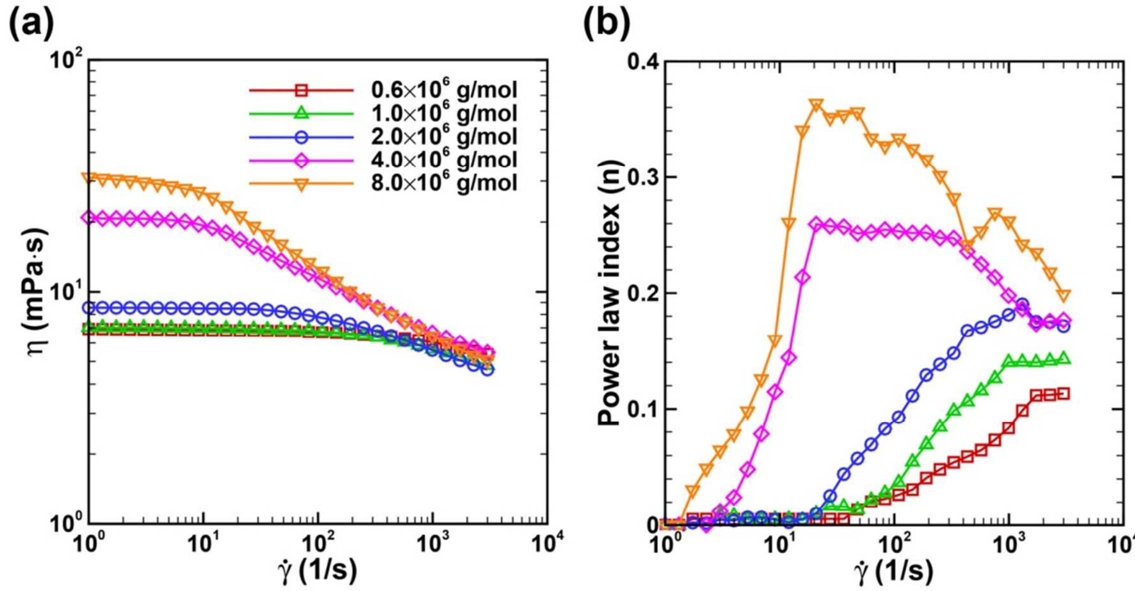

Figure S-4. (a) The measured shear viscosities of the PEO solutions with five different M_w for shear rates ranging from 1 to 3000 s^{-1}. (b) The shear thinning index n of power-law model against the shear rate. Here n is the absolute value of the slope of the shear-viscosity curve in the double-log Figure S-3(a).

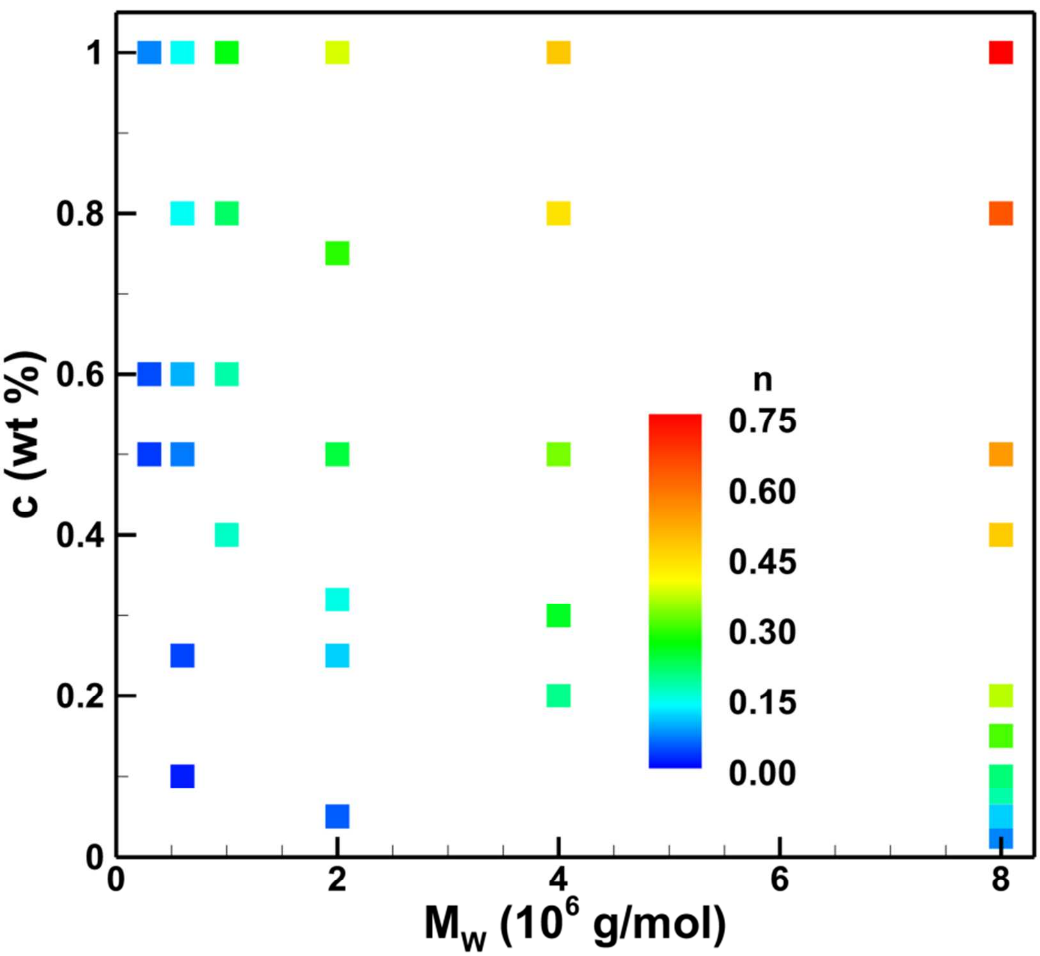

Figure S-5. The index *n* of power-law model $\eta \propto \dot{\gamma}^{-n}$ measured for PEO solutions of various M_w and c. Higher *n* indicates stronger shear thinning behavior. The *n* is determined by the data fitting of steady shear viscosities measured at the shear rates of 500-3000 s^{-1}.

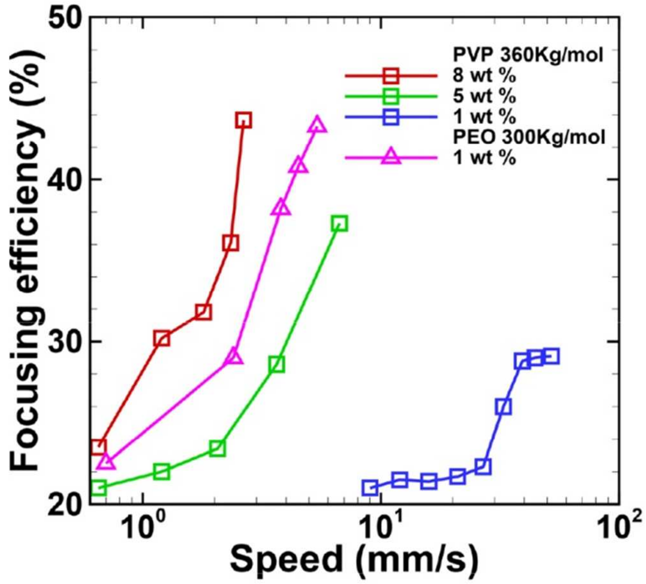

Figure S-6. The focusing efficiencies of 100 nm particles in 8 wt %, 5 wt %, and 1 wt % PVP solutions (M_w = 3.6×10^5 g/mol) and 1 wt % PEO solution (M_w = 3×10^5 g/mol) at various flow speeds.

ble S-2. Comparison of recent works on hydrodynamic focusing and separation using viscoelastic soluti

m particle r for successful ation (μm)	Minimum blockage ratio*	Sample flow rate (μL/h)	Focusing efficiency (%)	Separation efficiency (%)	Channel geometry and footprint	Journal	Man
	0.11	400-2000	> 95	N/A	Straight; N/A	Physical Review Letters	Visc
	0.116	5-2000	~100	N/A	Straight; 50 mm long	Nature Communications	Visc
	0.075	3×10^6	~90	N/A	Straight; 35 mm long	Nature Communications	Elast
	0.06	~O(100)	N/A	~100	Straight; 20 mm long	Analytical Chemistry	Elast fract
	0.063	10-100	~100	~100	Straight; 30 mm long	Analytical Chemistry	Elast focu
	0.038	~O(100)	N/A	~100	Spiral; 500 mm long	Scientific Reports	Visc
	0.053	600-4800	~100	~100	Straight; 48 mm long	Lab on a Chip	Elast focus
	0.1	30	N/A	~100	Straight; 25 mm long	Lab on a Chip	Elast focus
	0.118	40-320	N/A	> 95	Straight; 40 mm long	Lab on a Chip	Elast
	0.04	0.002-0.016	85	N/A	Straight; 100 mm long	Physical Review Applied	Visc
	0.04	< 0.96	Low: multiple streams	N/A	Straight; 40 mm long	Lab on a Chip	Visc
	0.04	~ 0.2	N/A	Low: only small portion of wanted particles flow into the collected outlet	Straight; ~1 mm long	Lab on a Chip	Hydr separ
	0.014	**0.32-2.45**	**84**	**> 95**	Double spiral; > 60 mm long; 3×3 mm^2		**Visc focus**

he smaller particles can be focused in a microchannel.

References

(1) Tirtaatmadja, V.; McKinley, G. H.; Cooper-White, J. J. *Phys. Fluids* **2006**, *18*, 043101.

(2) Rodd, L. E.; Scott, T. P.; Boger, D. V.; Cooper-White, J. J.; McKinley, G. H. *J. Non-Newton. Fluid Mech.* **2005**, *129*, 1-22.

(3) Doi, M.; Edwards, S. F. *The Theory of Polymer Dynamics*; Clarendon Press Oxford: Oxford, 1986.

(4) James, D. F. *Annu. Rev. Fluid Mech.* **2009**, *41*, 129-142.

(5) Morsi, S. A.; Alexander, A. J. *J. Fluid Mech.* **1972**, *55*, 193-208.

(6) Ho, B. P.; Leal, L. G. *J. Fluid Mech.* **1976**, *76*, 783-799.

(7) Leshansky, A. M.; Bransky, A.; Korin, N.; Dinnar, U. *Phys. Rev. Lett.* **2007**, *98*, 234501.

(8) Kang, K.; Lee, S. S.; Hyun, K.; Lee, S. J.; Kim, J. M. *Nat. Commun.* **2013**, *4*, 2567.

(9) Lim, E. J.; Ober, T. J.; Edd, J. F.; Desai, S. P.; Neal, D.; Bong, K. W.; Doyle, P. S.; McKinley, G. H.; Toner, M. *Nat. Commun.* **2014**, *5*, 4120.

(10) Lu, X.; Xuan, X. *Anal. Chem.* **2015**, *87*, 6389-6396.

(11) Liu, C.; Xue, C.; Chen, X.; Shan, L.; Tian, Y.; Hu, G. *Anal. Chem.* **2015**, *87*, 6041-6048.

(12) Lee, D. J.; Brenner, H.; Youn, J. R.; Song, Y. S. *Sci. Rep.* **2013**, *3*, 3258.

(13) Yuan, D.; Zhang, J.; Sluyter, R.; Zhao, Q.; Yan, S.; Alici, G.; Li, W. *Lab Chip* **2016**, *16*, 3919-3928.

(14) Nam, J.; Lim, H.; Kim, D.; Jung, H.; Shin, S. *Lab Chip* **2012**, *12*, 1347-1354.

(15) Yang, S.; Kim, J. Y.; Lee, S. J.; Lee, S. S.; Kim, J. M. *Lab Chip* **2011**, *11*, 266-273.

(16) De Santo, I.; D’Avino, G.; Romeo, G.; Greco, F.; Netti, P. A.; Maffettone, P. L. *Phys. Rev. Applied* **2014**, *2*, 064001.

(17) Kim, J. Y.; Ahn, S. W.; Lee, S. S.; Kim, J. M. *Lab Chip* **2012**, *12*, 2807-2814.

(18) Fouet, M.; Mader, M. A.; Irain, S.; Yanha, Z.; Naillon, A.; Cargou, S.; Gue, A. M.; Joseph, P. *Lab Chip* **2016**, *16*, 720-733.